Supporting Information

A Dinitrophenol-Based Colorimetric Chemosensor for Sequential Cu^{2+} And S^{2-} Detection

Hyejin Nam, Sungjin Moon *, Dongkyun Gil, Cheal Kim *

Department of Fine Chemistry and Renewable Energy Convergence, Seoul National University of Science and Technology (SNUT), Seoul 01098, Korea.

Correspondence: msjinjjang@naver.com (S. M.); chealkim@snut.ac.kr (C.K.)

Table S1. Examples of chemosensors for sequential detecting of Cu^{2+} and S^{2-} through color variation in aqueous solution.

Sensor	Solvent	Detection limit for Cu^{2+} (μM)	Detection limit for S^{2-} (μM)	Reference
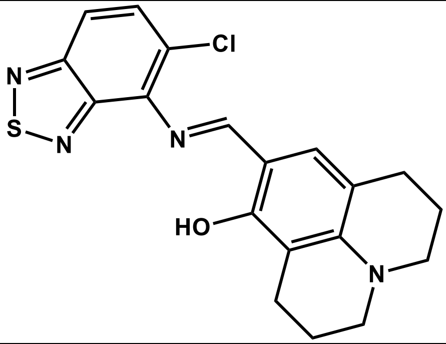	MeOH:H_2O 90:10	5.5×10^{-1}	4.5×10^{-1}	[1]
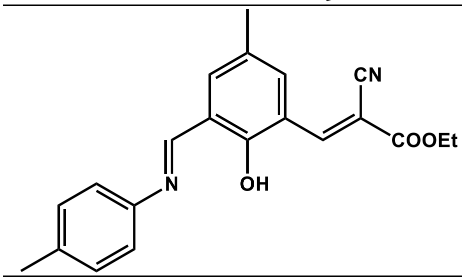	CH_3CN:H_2O 80:20	-	-	[36]
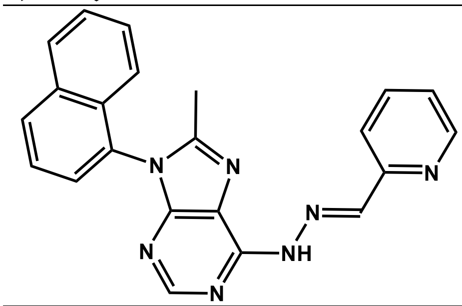	DMSO:H_2O 60:40	7.5×10^{-2}	2.0	[37]
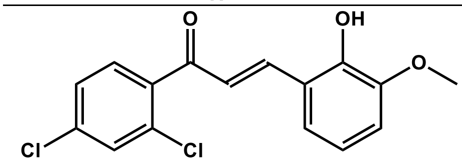	CH_3CN:H_2O 50:50	1.3	4.0×10^{-1}	[31]
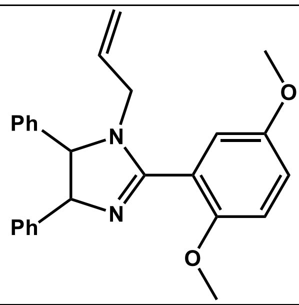	IPA:H_2O 50:50	3.3×10^{-1}	1.9	[53]

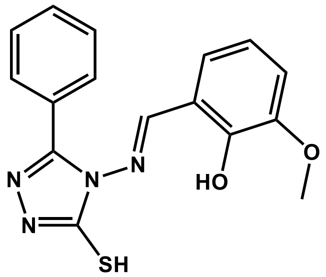	$CH_3CN:H_2O$ 50:50	1.1×10^{-1}	2.3×10^{-1}	[35]
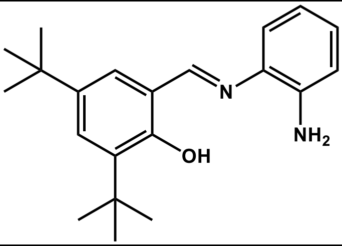	$DMSO:H_2O$ 50:50	1.2×10^{-1}	1.7	[30]
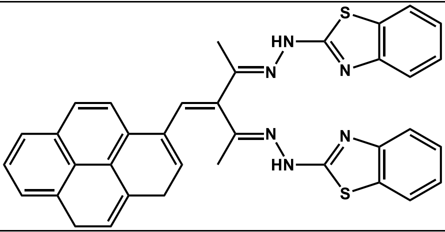	$DMSO:H_2O$ 20:80	-	-	[21]
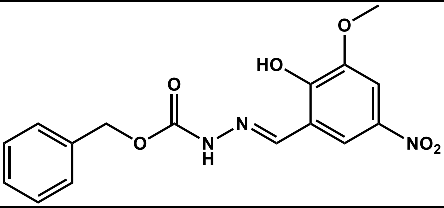	$H_2O:DMSO$ 99:1	2.0×10^{-1}	6.0×10^{-1}	[34]
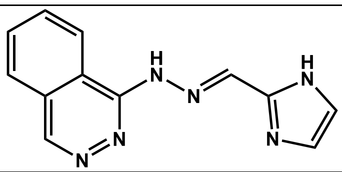	$H_2O:MeOH$ 99.7:0.3	1.2×10^{-1}	8.0×10^{-1}	[57]
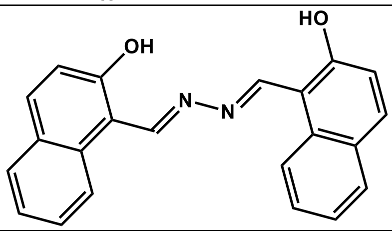	$H_2O:DMSO$ 99.95 : 0.05	-	-	[33]
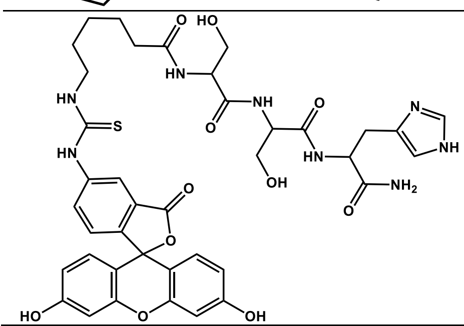	H_2O 100	-	-	[32]

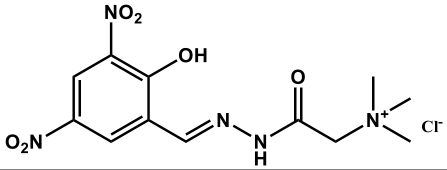	H_2O:DMSO 99.9:0.1	6.4×10^{-2}	1.2×10^{-1}	This work

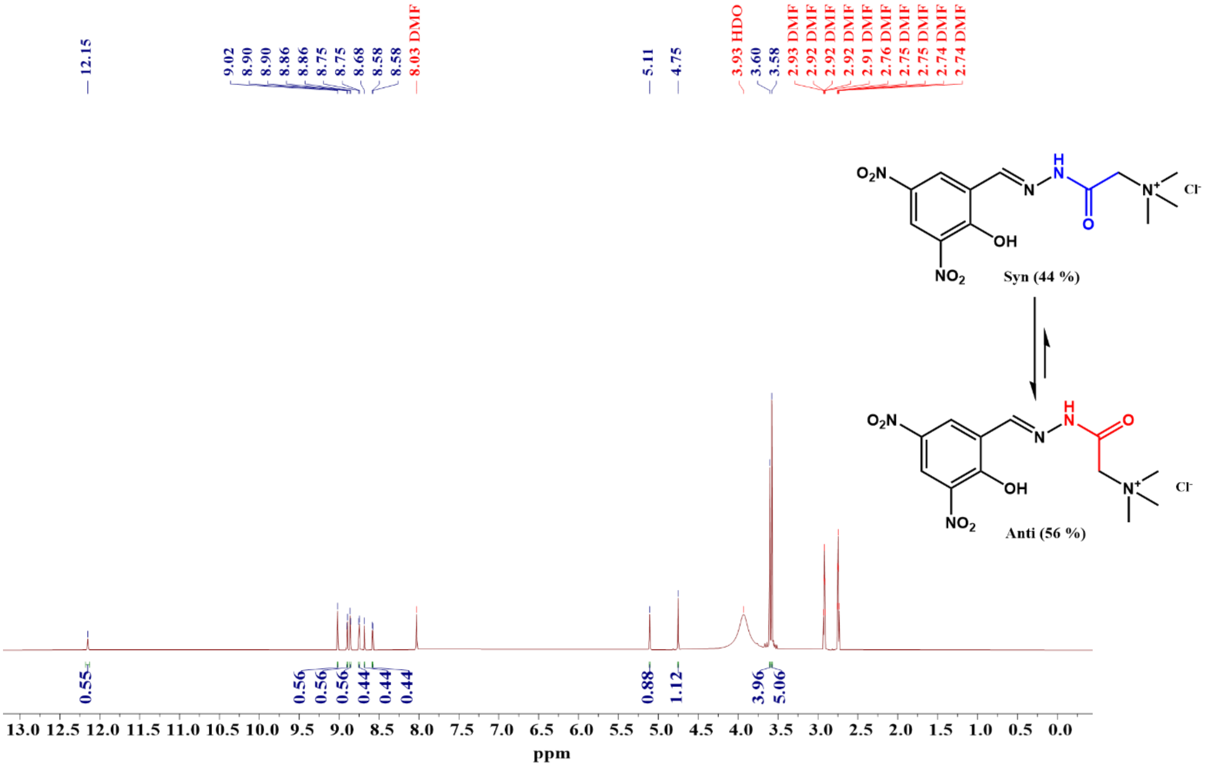

Figure S1. ^{1}H NMR spectrum of **HDHT**.

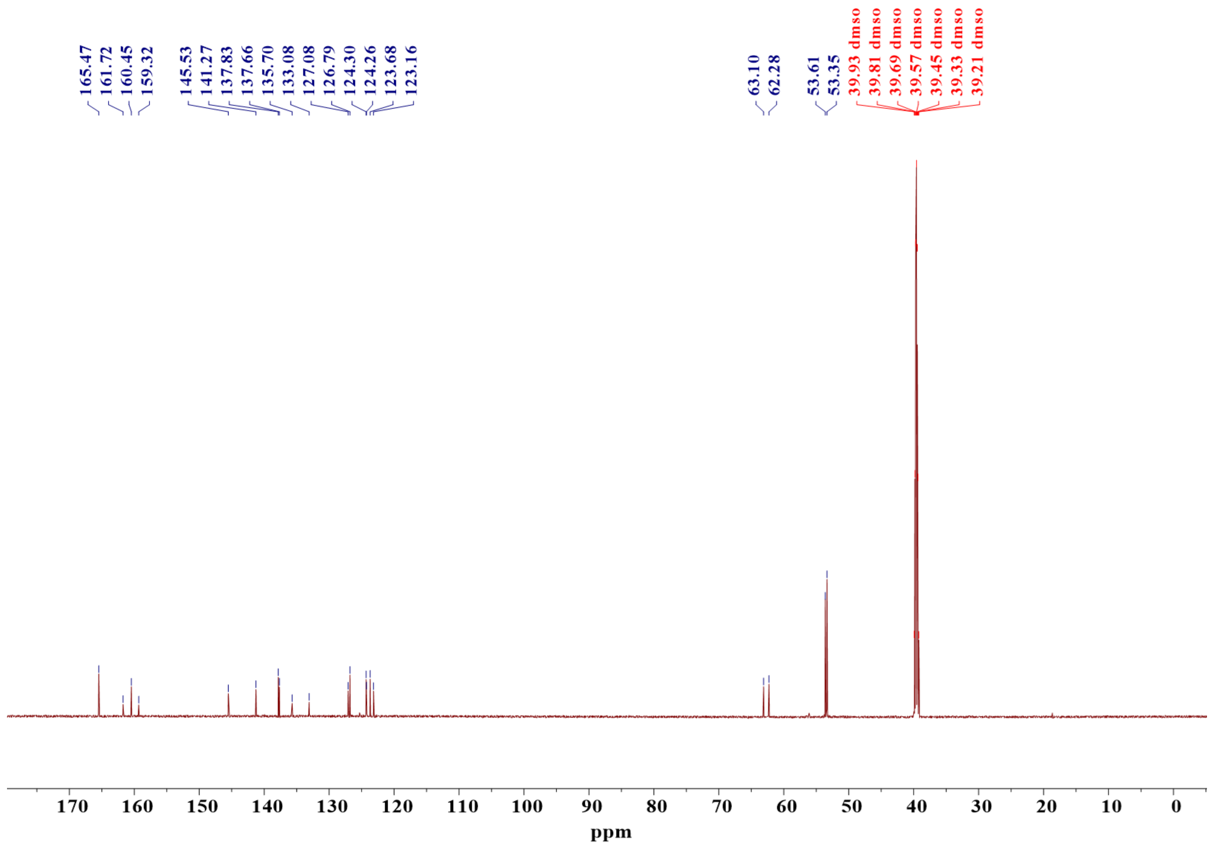

Figure S2. ^{13}C NMR spectrum of **HDHT**.

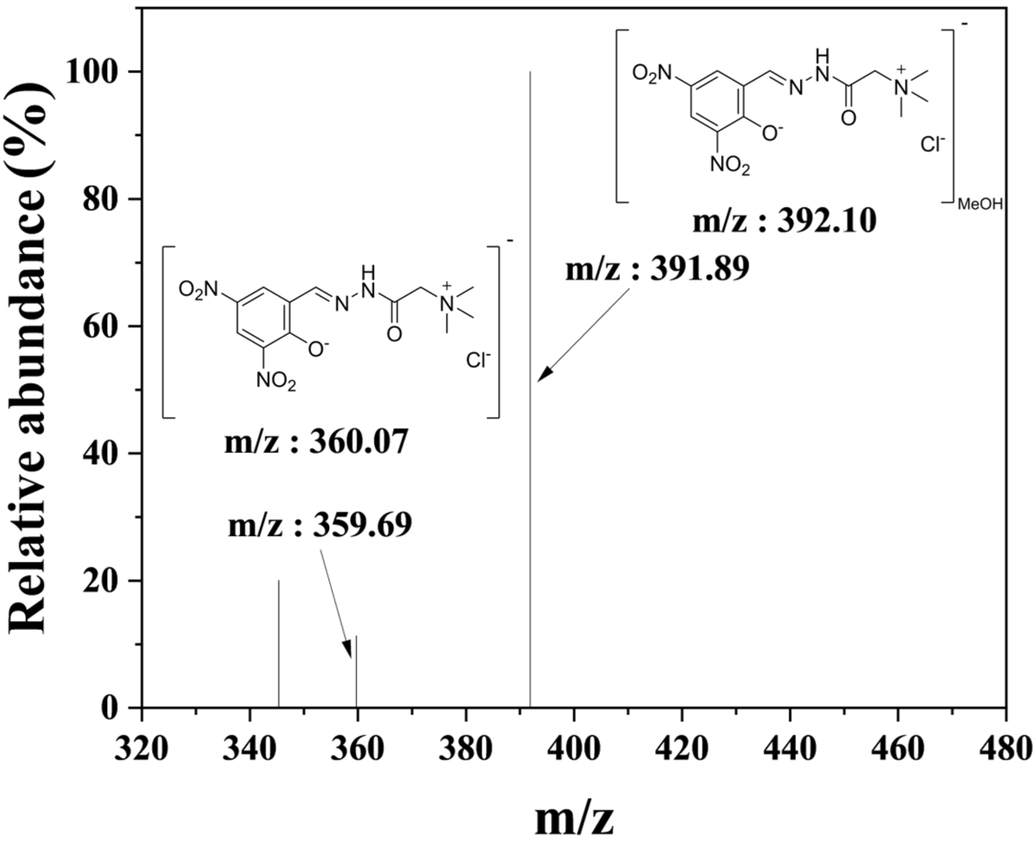

Figure S3. Negative ion ESI-MS spectra of **HDHT** (100 μM).

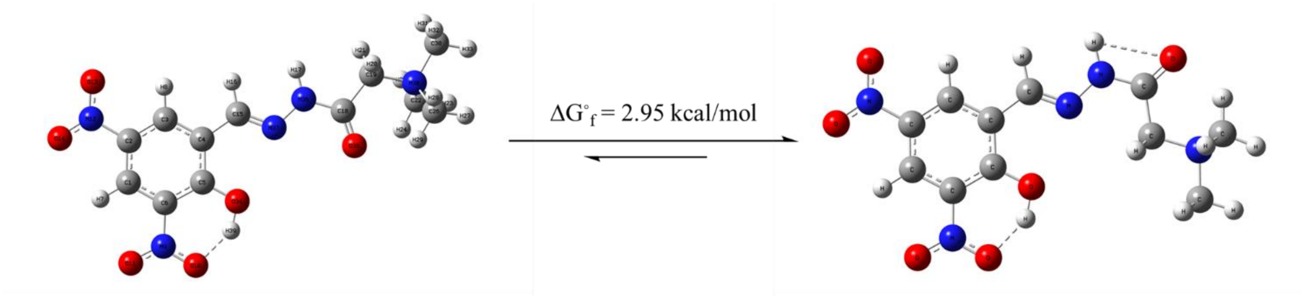

syn isomer
-747627.12 kcal/mol

anti isomer
-747630.07 kcal/mol

Figure S4. Gibbs free-energy ($\Delta G°_f$) calculation for optimized isomers of **HDHT**.

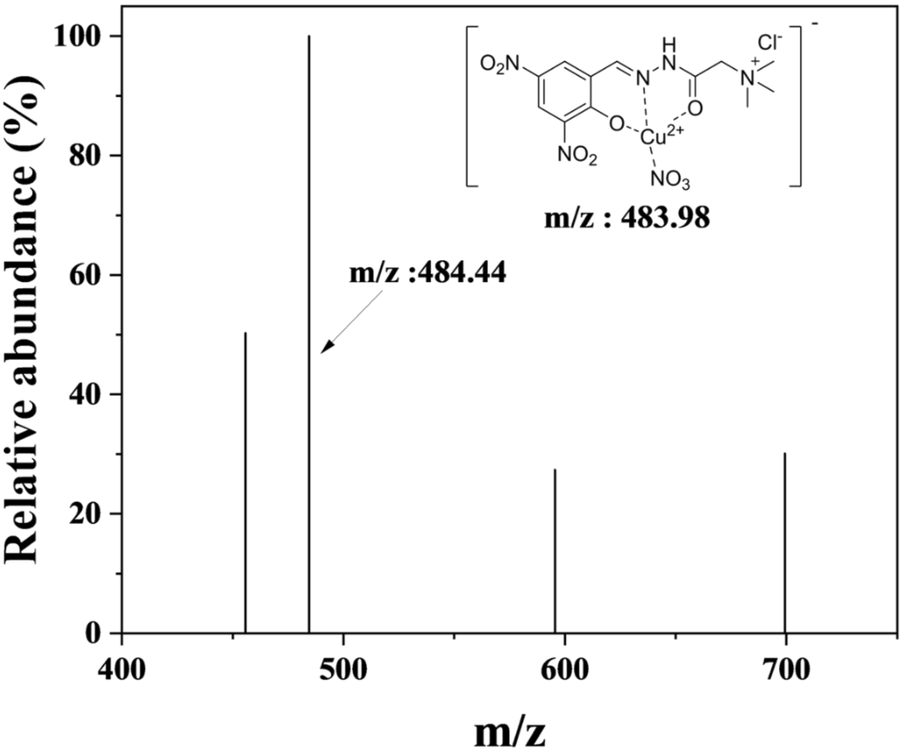

Figure S5. Negative ion ESI-MS spectra of **HDHT** (100 μM) with Cu^{2+} (100 μM).

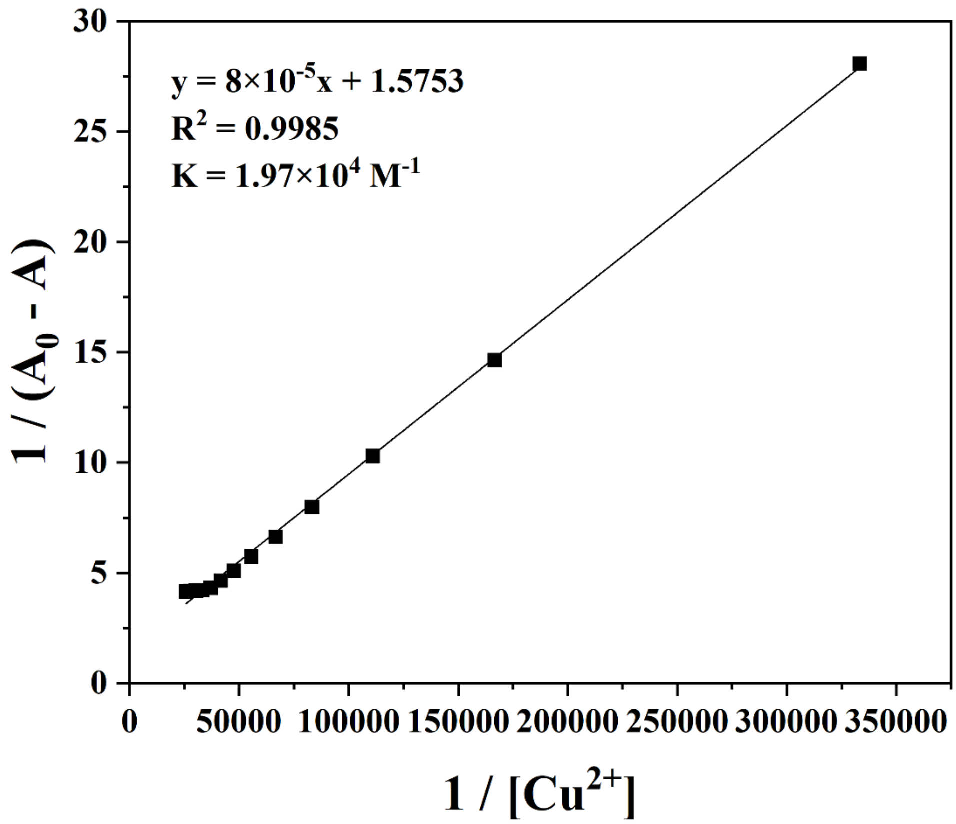

Figure S6. The binding constant of **HDHT** (30 μM) with Cu^{2+} by using the Benesi-Hildebrand method. The absorbance spectrum at 430 nm is measured by the increasing equivalent of Cu^{2+}.

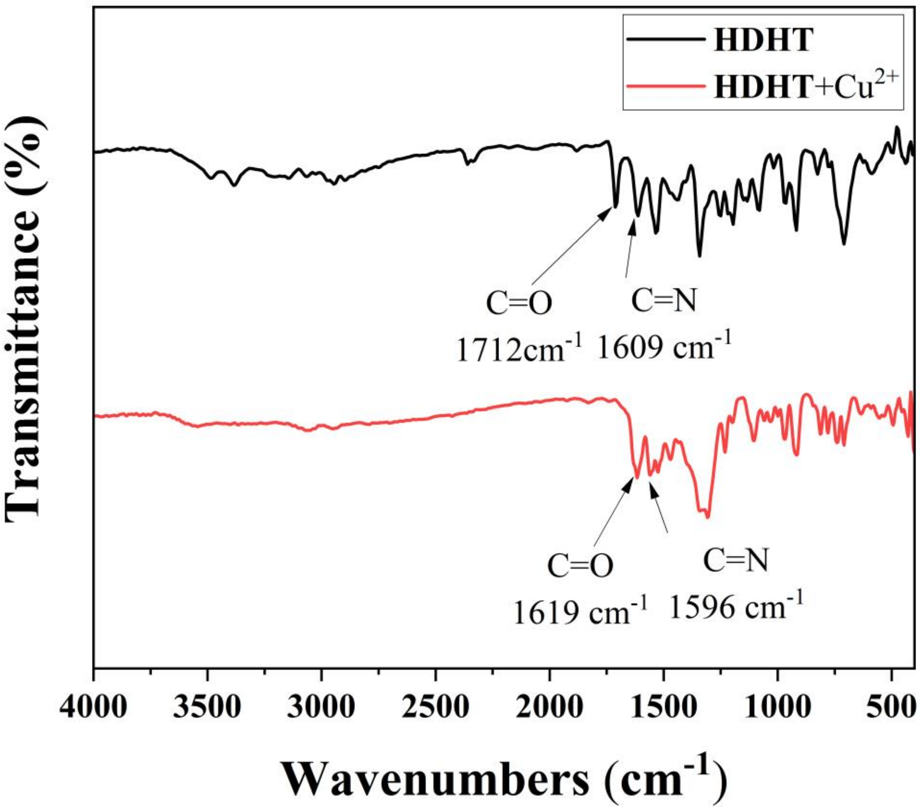

Figure S7. FT-IR spectra of **HDHT** (black line) and **HDHT**-Cu^{2+} (red line).

(a)

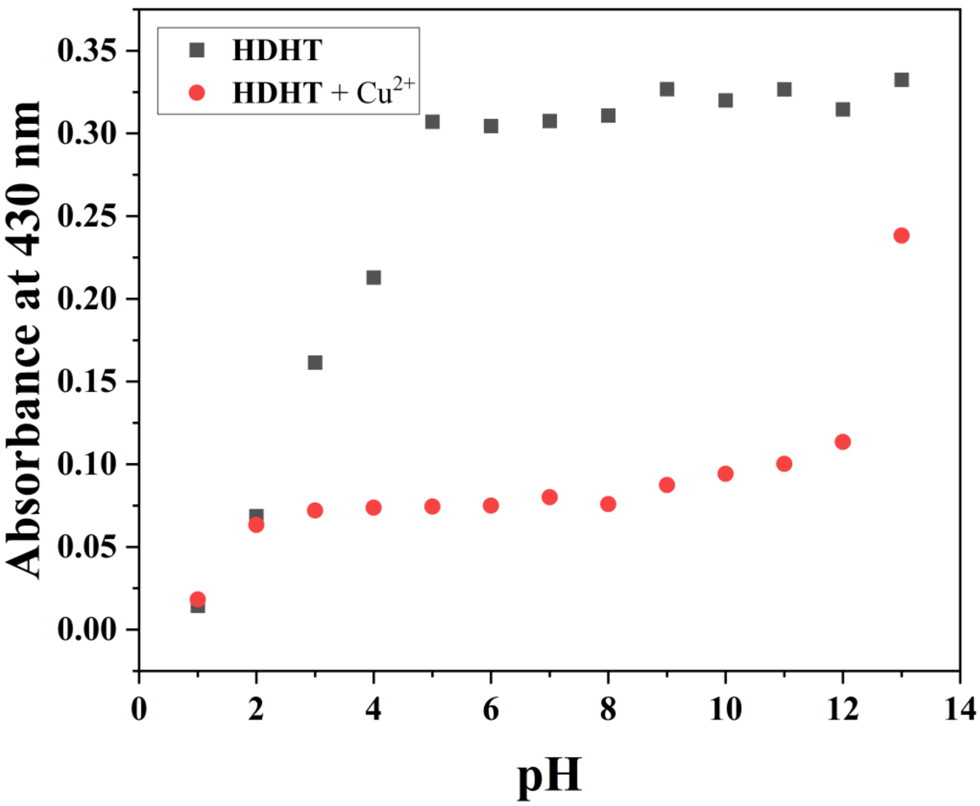

(b)

Figure S8. pH stability test. (a) UV-vis absorbance at 430 nm of **HDHT** (30 μM) and **HDHT**-Cu^{2+} (30 μM) in buffer solution from pH 1 to pH 13. (b) Color change of **HDHT** (30 μM) and **HDHT**-Cu^{2+} (30 μM) in buffer solution from pH 1 to pH 13.

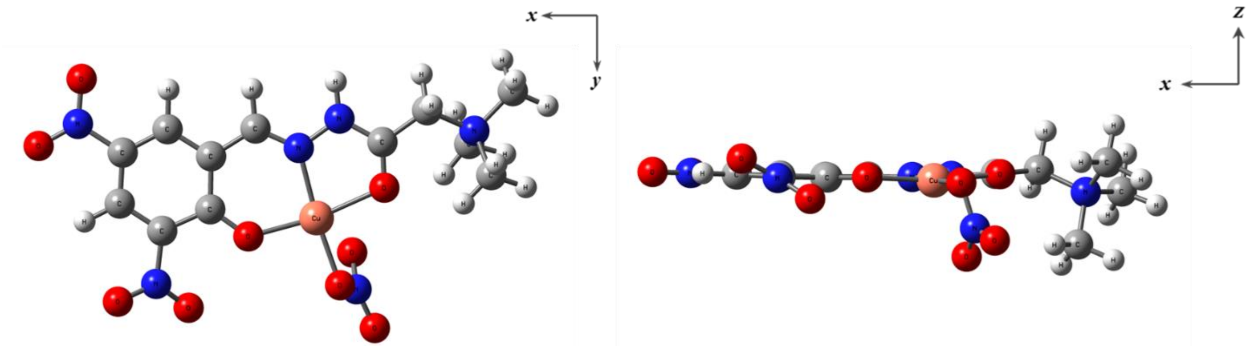

Figure S9. Energy-optimized structure of **HDHT**-Cu^{2+} complex.

(a)

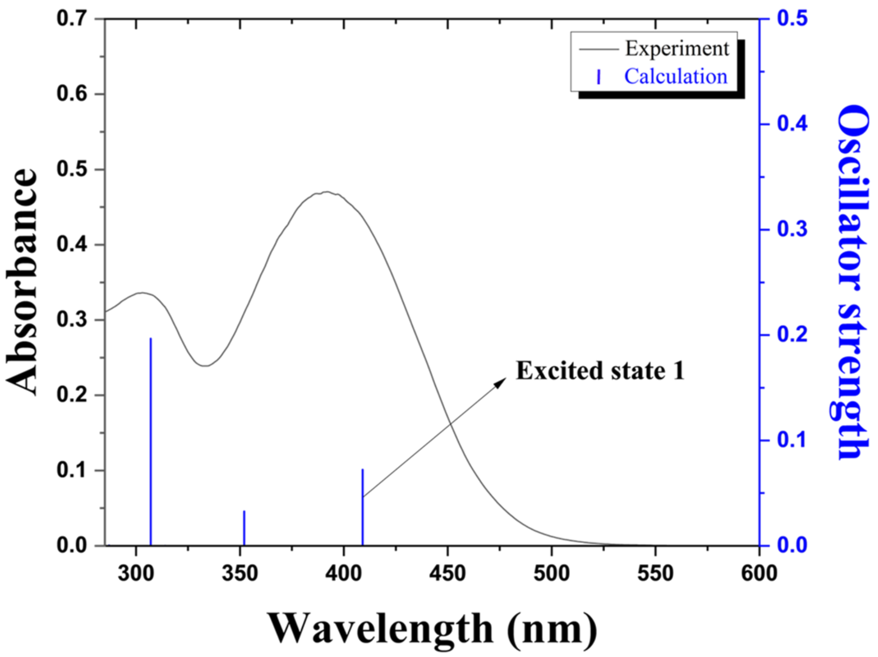

(b)

Excited state 1	Wavelength	Percent	Main Character	Oscillator strength
H → L	409.32 nm	99 %	ICT	0.0723

Figure S10. (a) The theoretical excitation energies and the experimental UV-vis spectrum of **HDHT**. (b) The major electronic transition energies and molecular orbital contributions for **HDHT** (H = HOMO and L = LUMO).

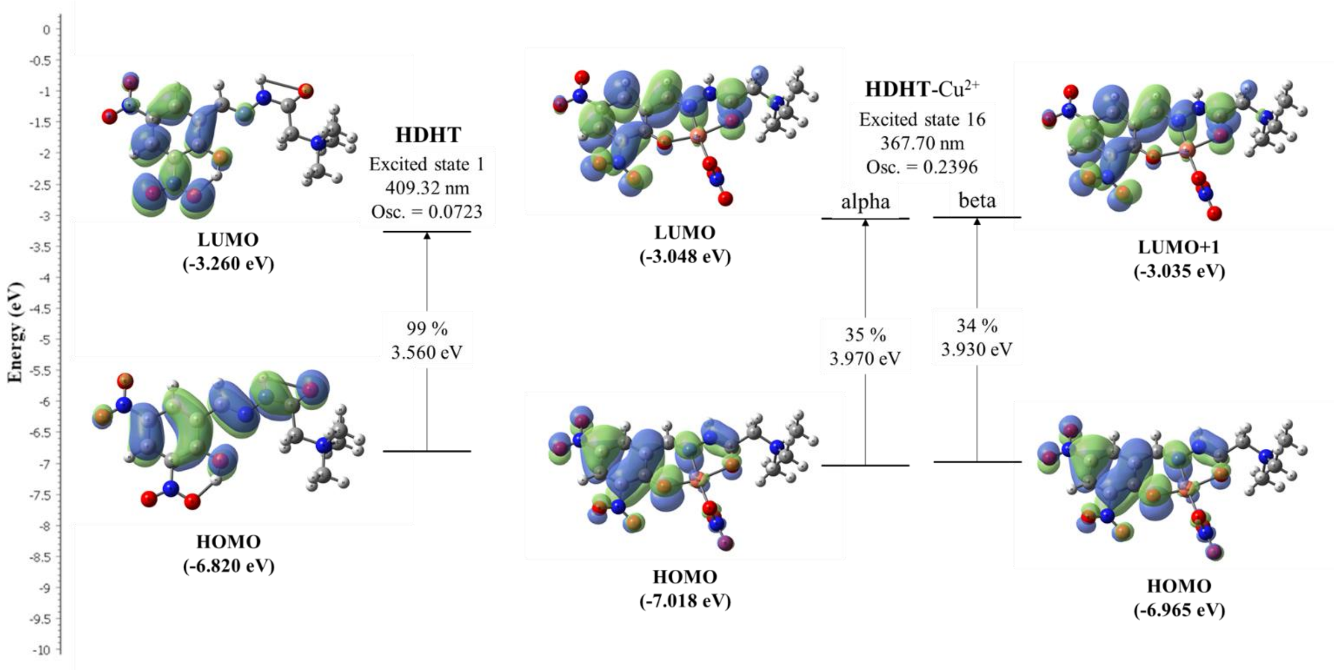

Figure 11. Molecular orbital diagrams and excitation energies of **HDHT** and **HDHT**-Cu^{2+}.

(a)

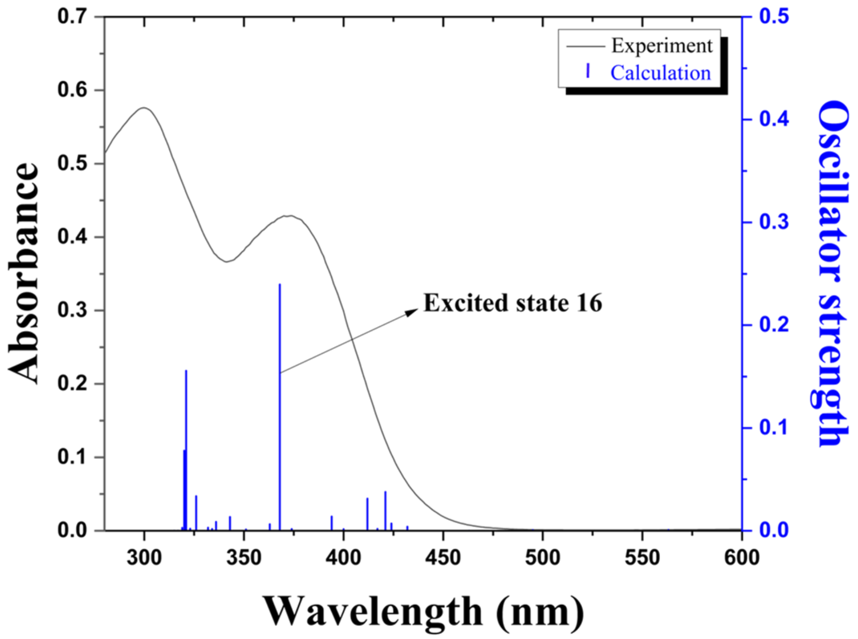

(b)

Excited state 16	Wavelength	Percent	Main Character	Oscillator strength
H → L (alpha)	367.70 nm	35 %	$\pi \rightarrow \pi^*$	0.2396
H → L+1 (beta)		34 %	$\pi \rightarrow \pi^*$	

Figure 12. (a) The theoretical excitation energies and the experimental UV-vis spectrum of **HDHT**-Cu^{2+}. (b) The major electronic transition energies and molecular orbital contributions for **HDHT**-Cu^{2+} (H = HOMO and L = LUMO).

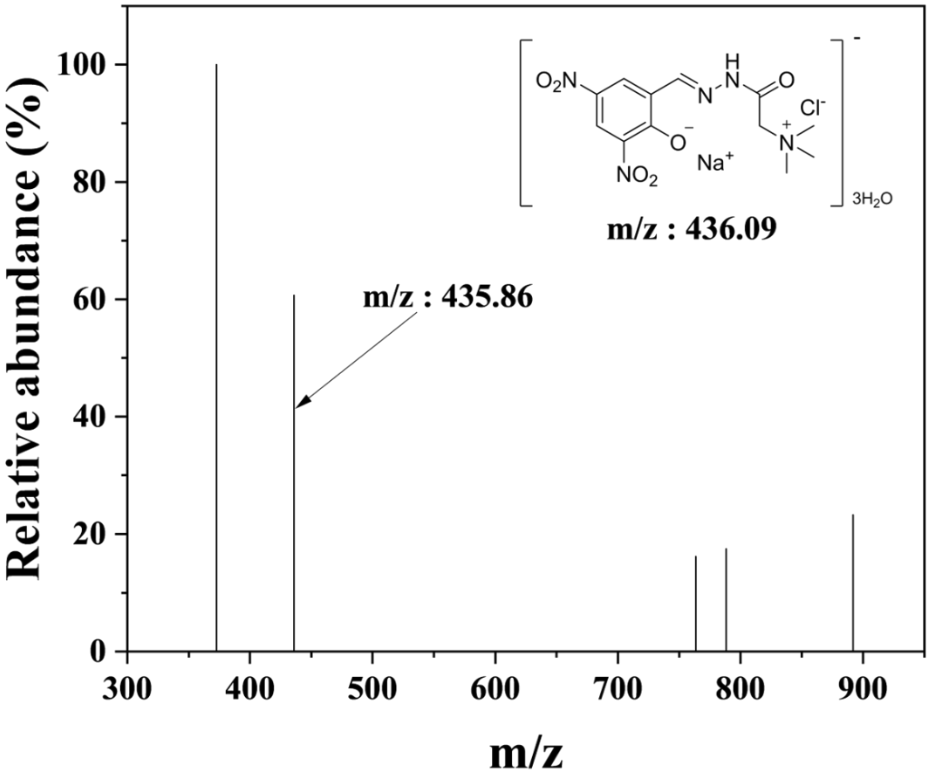

Figure S13. Negative ion ESI-MS spectra of **HDHT-**Cu^{2+} (100 μM) with S^{2-} (100 μM).

(a)

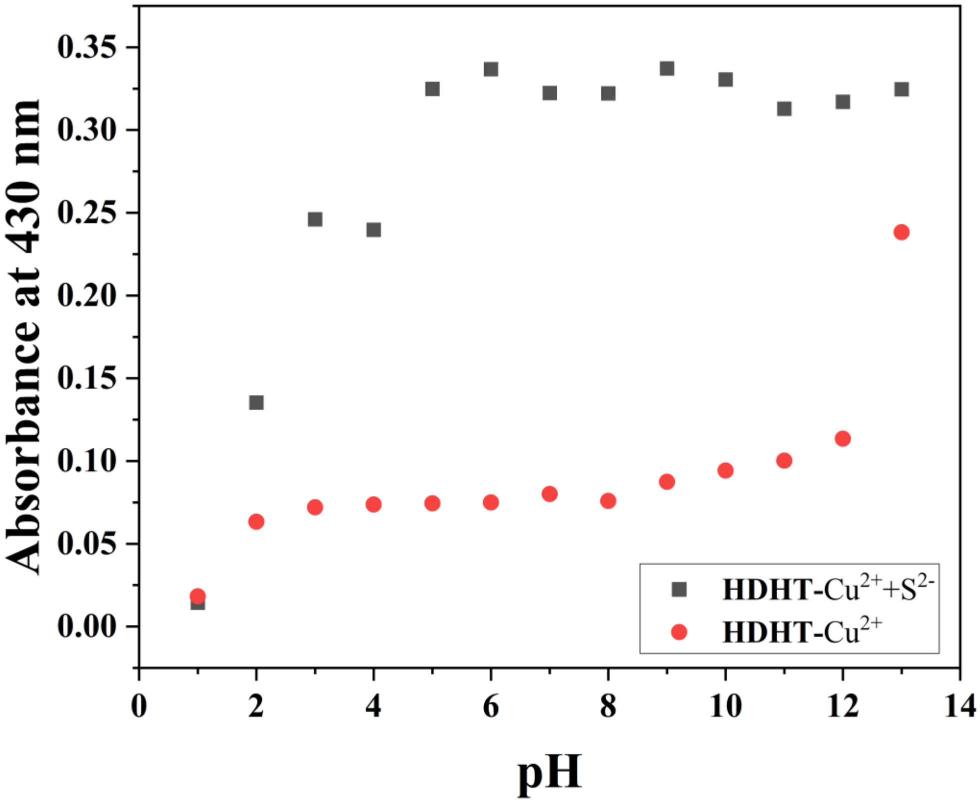

(b)

Figure S14. pH stability test. (a) UV-vis absorbance at 430 nm of **HDHT**-Cu^{2+} (30 μM) and **HDHT**-Cu^{2+} + S^{2-} (30 μM) in buffer solution from pH 1 to pH 13. (b) Color change of **HDHT**-Cu^{2+} (30 μM) and **HDHT**-Cu^{2+} + S^{2-} (30 μM) in buffer solution from pH 1 to pH 13.